Effects of neonatal amygdala or hippocampus lesions on resting brain metabolism in the macaque monkey: A microPET imaging study

Christopher J. Machado,[a,b] Abraham Z. Snyder,[c] Simon R. Cherry,[d] Pierre Lavenex,[a,b,e] and David G. Amaral[a,b,*]

[a]*Department of Psychiatry and Behavioral Sciences, the California National Primate Research Center, 2825 50th Street, UC Davis, Sacramento, CA 95817, USA*
[b]*The M.I.N.D. Institute, 2825 50th Street, UC Davis, Sacramento, CA 95817, USA*
[c]*Department of Radiology, Washington University School of Medicine, St. Louis, MI 63110, USA*
[d]*Department of Biomedical Engineering, Center for Molecular and Genomic Imaging, 1 Shields Ave, UC Davis, Davis, CA 95616, USA*
[e]*Department of Medicine, Unit of Physiology, University of Fribourg, Chemin du Musée 5, CH-1700 Fribourg, Switzerland*

Longitudinal analysis of animals with neonatal brain lesions enables the evaluation of behavioral changes during multiple stages of development. Interpretation of such changes, however, carries the caveat that permanent neural injury also yields morphological and neurochemical reorganization elsewhere in the brain that may lead either to functional compensation or to exacerbation of behavioral alterations. We have measured the long-term effects of selective neonatal brain damage on resting cerebral glucose metabolism in nonhuman primates. Sixteen rhesus monkeys (*Macaca mulatta*) received neurotoxic lesions of either the amygdala ($n=8$) or hippocampus ($n=8$) when they were two weeks old. Four years later, these animals, along with age- and experience-matched sham-operated control animals ($n=8$), were studied with high-resolution positron emission tomography (microPET) and 2-deoxy-2 [^{18}F]fluoro-D-glucose ([^{18}F]FDG) to detect areas of altered metabolism. The groups were compared using an anatomically-based region of interest analysis. Relative to controls, amygdala-lesioned animals displayed hypometabolism in three frontal lobe regions, as well as in the neostriatum and hippocampus. Hypermetabolism was also evident in the cerebellum of amygdala-lesioned animals. Hippocampal-lesioned animals only showed hypometabolism in the retrosplenial cortex. These results indicate that neonatal amygdala and hippocampus lesions induce very different patterns of long-lasting metabolic changes in distant brain regions. These observations raise the possibility that behavioral alterations in animals with neonatal lesions may be due to the intended damage, to consequent brain reorganization or to a combination of both factors.

The study of neurodevelopmental disorders within a clinical setting is inherently complex since each patient's specific behavioral and cognitive deficits stem from a unique interaction between genetic, neurobiological and environmental factors. Longitudinal analysis of animal models provides a complementary approach, since genetic, neurobiological and environmental factors can be selectively manipulated and tightly controlled. For example, nonhuman primates have been commonly used to investigate the behavioral consequences of neonatal brain damage through multiple stages of development (Goldman-Rakic, 1987; Alvarado and Bachevalier, 2000; Machado and Bachevalier, 2003; Bauman and Amaral, 2007). However, brain injury in developing individuals yields morphological and neurochemical reorganization that may, along with the lesion, either exacerbate or mitigate behavioral deficits. Neonatal medial temporal lobe lesions, for example, result in delayed maturation of the dorsolateral prefrontal cortex (Bertolino et al., 1997), which subsequently leads to dysregulation of striatal domaminergic neurotransmission (Saunders et al., 1998; Heinz et al., 1999). By contrast, structural reorganization and functional compensation may explain why humans and monkeys with early hippocampal damage demonstrate intact semantic and spatial memory (Vargha-Khadem et al., 1997; Lavenex et al., 2007), but individuals with similar damage occurring in adulthood exhibit severe memory deficits (Zola et al., 1986; Rempel-Clower et al., 1996; Banta-Lavenex et al., 2006).

High-resolution positron emission tomography (microPET) provides a powerful, noninvasive means to visualize neural activity in animals (Tai et al., 2001), including the metabolic sequelae following selective brain damage. For example, adult rodents and monkeys with lesions of the basal forebrain (Le Mestric et al., 1998; Katsumi et al., 1999), or the entorhinal or perirhinal cortices (Hayashi et al., 1999; Meguro et al., 1999; Millien et al., 2002; Rauchs et al., 2006) have demonstrated altered glucose metabolism within brain areas that are heavily interconnected with the lesion site. Although these results indicate that lesions in the mature primate brain can significantly alter the activity of undamaged

* Corresponding author. The M.I.N.D. Institute, University of California, Davis, 2825 50th Street, Sacramento, CA 95817, USA. Fax: +1 916 703 0287.
E-mail address: dgamaral@ucdavis.edu (D.G. Amaral).

regions, it is unclear if lesions during infancy result in more drastic metabolic alterations or if structural reorganization can partially or fully compensate for the damage. Furthermore, when multiple scans have been acquired in the months following adult brain lesions, there have been indications of partial metabolic recovery (Le Mestric et al., 1998; Hayashi et al., 1999; Katsumi et al., 1999; Moore et al., 2000; Millien et al., 2002; Rauchs et al., 2006). A more stable picture of how selective lesions affect cerebral metabolism would materialize if animals were scanned several years post-lesion, but such a study has not yet been conducted.

The goal of the current study was to use microPET imaging to noninvasively measure resting brain metabolism in adult (4-year-old) rhesus monkeys that had received bilateral neurotoxic amygdala or hippocampus lesions shortly after birth. We hypothesized that both lesions would lead to hypometabolism in areas with which the lesioned brain regions share substantial monosynaptic connections. Given previous autoradiographic evidence with rats (Gerrits et al., 2006), we also predicted that hypometabolism would be more extensive following amygdala lesions than following damage to the hippocampus. To test these hypotheses, we analyzed anatomically-defined ROIs to compare relative glucose metabolism outside the lesion target between each operated group and a group of age- and experienced-matched sham-operated control animals. A preliminary report of this work has appeared previously in abstract form (Machado et al., 2006).

Materials and methods

All experimental procedures were developed in collaboration with the veterinary staff at the California National Primate Research Center (CNPRC). All protocols were approved by the University of California, Davis, Institutional Animal Care and Use Committee.

Subjects and rearing conditions

Twenty-four rhesus monkeys (*Macaca mulatta*) were studied. These animals were naturally born of multiparous mothers and were randomly assigned to one of three lesion conditions: Sham-operated control (CON; $n=8$; four females, four males), bilateral ibotenic acid hippocampus lesion (HIP; $n=8$; five females, three males), and bilateral ibotenic acid amygdala lesion (AMY; $n=8$; five females, three males). All surgeries occurred when animals were 11–18 days old. Animals were returned to their mothers following surgery and were provided with a social rearing environment described in detail previously (Bauman et al., 2006). Briefly, beginning approximately 14 days after surgery, each experimental animal and its mother were allowed daily access to a socialization group consisting of five other mother–infant pairs and one adult male. A total of four such socialization groups were formed, and each interacted for a minimum of 3 h per day, 5 days per week. At 6 months of age, infants were permanently separated from their mothers, but continued to experience the same socialization schedule and partners, with the addition of an unfamiliar adult female. At 1 year of age, all animals became permanently socially housed (24 h per day) with the five peers, adult male and adult female from their socialization groups in one of four chain-link, indoor enclosures (2.13 m width × 3.35 m length × 2.44 m height). Over the next 4 years, all animals were studied in a range of behavioral tasks, including assessments of social behavior (Prather et al., 2001; Bauman et al., 2004a, 2006), maternal preference (Bauman et al., 2004a), spatial relational memory (Lavenex et al., 2007), and emotional reactivity.

The current study was conducted when the animals were between 3.9 and 4.8 years old, weighed 5.1–10.1 kg and were not participating in any other behavioral testing. Animals were removed from their socialization groups 1–3 months prior to the current study and housed indoors within two adjoining cages (each 66 cm width × 61 cm length × 81 cm height) in same sex pairs. The housing room was maintained on a 12 h light/dark cycle. Animals were fed fresh fruit, vegetables and high-protein monkey chow (Lab Diet #5047, PMI Nutrition International Inc., Brentwood, MO) daily and received water *ad libitum*.

Surgical procedures

A detailed description of all surgical procedures can be found elsewhere (Bauman et al., 2004a, 2006). In brief, the animals were anesthetized with ketamine hydrochloride (15 mg/kg i.m.) and medetomidine (30 μg/kg), and placed in an MRI-compatible stereotaxic frame (Crist Instruments Co., Inc., Damascus, MD). A T1-weighted MRI series was acquired to determine the location of the amygdala or hippocampus and calculate three-dimensional coordinates for ibotenic acid injections. Infants were then transported to the surgical suite without removal from the stereotaxic frame. Animals were ventilated and vital signs monitored by CNPRC veterinary staff throughout the surgery. Anesthesia and analgesia were maintained using a combination of isoflurane gas (~1%) and intravenous infusion of fentanyl (7–10 μg/kg/h). Following a midline incision, the skin was reflected laterally to expose the skull, two craniotomies were made over the amygdala or the hippocampus depending on the pre-determined lesion condition, and the dura was reflected to expose the surface of the brain. Ibotenic acid (Biosearch Technologies Inc., 10 mg/ml in 0.1 M phosphate buffered saline) was simultaneously injected bilaterally into the amygdala or hippocampus (the dentate gyrus, CA1–CA3 fields of the hippocampus and the subiculum) using 10 μl Hamilton syringes (26 gauge beveled needles) at a rate of 0.2 μl/min. Following all injections, the wound was closed in anatomical layers. Sham-operated controls underwent the same surgical procedures (including midline incision, skull exposure and wound closure) and were maintained under anesthesia for the average duration of the lesion surgeries. Following surgery, all infants were monitored by a CNPRC veterinarian and returned to their mothers once they were fully alert. The approximate extent of the lesion was visualized in each case using T2-weighted MR images acquired 10 days post-surgery. This type of MR image is particularly sensitive to edema associated with neurotoxin-induced cell death. The methods for these scans have been described in detail elsewhere (Bauman et al., 2004a, 2006).

Neuroimaging

MRI

At approximately 4 years post-surgery, each animal received an additional T1-weighted structural MRI scan. Animals were anesthetized with ketamine hydrochloride (15 mg/kg i.m.) and medetomidine (25–50 μg/kg) throughout the entire procedure. Opthalmic ointment (Puralube; Pharmaderm Animal Health, Melville, NY) was placed in the animals' eyes to prevent drying. The animal's head was secured in an MRI-compatible stereotaxic frame (Crist Instruments Co., Inc.) and centered with respect to the

magnet. All MRI scans were performed with a 1.5 Tesla scanner (Genesis Signa model, General Electric Medical Systems, Milwaukee, WI) and a human head coil that surrounded the stereotaxic frame. Approximately 80 1.0-mm-thick images were acquired using a T1-weighted spoiled gradient (SPGR) pulse sequence (repetition time=22 ms; echo time=7.9 ms; number of excitations=4; field of view (FOV)=16 cm; matrix=256×256).

These high-resolution MRI scans served two important functions. First, these images were used to measure the extent of each animal's lesion, since these animals are still involved in behavioral experiments. The Analyze software ROI tool (v. 8.0; Mayo Clinic via AnalyzeDirect, Lenexa, KS) was used to measure the volume (in mm^3) of the left and right hippocampus and amygdala in each of the sham-operated and lesioned animals. Anatomical boundaries for each structure on MR images are described in the Supplementary Materials section online. Volumetric data from the eight sham-operated animals were averaged, and used to estimate the percentage of hippocampal or amygdaloid tissue atrophy: Percent Reduction=((Control Mean Volume−Lesioned-Animal Volume)/Control Mean Volume)×100. The MRI scans also served as individualized anatomical references for each animal, upon which specific ROIs could be reliably drawn and used for measuring metabolic data on registered microPET volumes (see Data analysis).

MicroPET

To measure resting cerebral glucose metabolism, a correlate of synaptic activity (Sokoloff, 1999), each animal received a single microPET imaging session following intravenous infusion of 2-deoxy-2[^{18}F]fluoro-D-glucose ([^{18}F]FDG; PETNET Radiopharmaceuticals, Sacramento, CA). All animals were initially immobilized in their living quarters with ketamine hydrochloride (10 mg/kg) and given atropine (0.04 mg/kg) to maintain heart rate. After being transported to an animal preparation room, animals were intubated with an endotracheal canula for isoflurane sedation (1–2%) during the imaging session. Although several previous studies have demonstrated that ketamine (Holcomb et al., 2001; Langsjo et al., 2003, 2004; Freo and Ori, 2004; Honey et al., 2004; Itoh et al., 2005) and isoflurane (Maekawa et al., 1986; Ori et al., 1986; Alkire et al., 1997; Shimoji et al., 2004; Toyama et al., 2004) anesthesia can affect cerebral metabolism and regional cerebral blood flow in rodents, monkeys and humans, the affects appear to be constant across subjects within a given study. Since all animals underwent the same protocol, anesthesia per se should not induce group differences in glucose metabolism. Moreover, since isoflurane typically reduces cerebral metabolism relative to the non-anesthetized state (Noda et al., 2003; Shimoji et al., 2004), the differences between groups reported here may be underestimates of the actual differences.

An intravenous catheter was placed in the right cephalic vein for acquiring a blood sample, infusion of [^{18}F]FDG and delivery of fluids (lactated Ringer's solution). Opthalmic ointment was again placed in the animals' eyes to prevent drying. A 1 ml blood sample was collected prior to infusion of [^{18}F]FDG. This was used to determine if any animal differed significantly in circulating blood glucose levels which could potentially affect [^{18}F]FDG uptake into the brain. The blood sample was allowed to clot at room temperature and centrifuged at 3000 revolutions per minute (RPM). The serum was separated and stored at −80 °C until glucose concentrations were determined in a standard serum chemistry profile.

Each animal was then transported to the microPET Imaging Facility at the CNPRC and placed in a supine position on a microPET scanner bed (Model P4, Siemens Preclinical Solutions, Knoxville, TN—formerly Concorde Microsystems, LLC, Tai et al., 2001). This scanner has a 22 cm animal port, a 19 cm transaxial FOV and 7.8 cm axial FOV. The animal's head was secured to the scanner bed using self-adherent wrap (Vetrap, 3M, St. Paul, MN) and centered within the animal port using a laser positioning system. A veterinarian monitored anesthesia level, heart rate, blood oxygenation and CO_2 levels throughout the entire procedure.

Approximately 15 min after sedation in the living quarters, [^{18}F]FDG (1.7–2.3 mCi; 150–400 μl) was infused via the intravenous catheter. The emission scan (45-min duration, 3-D data acquisition mode) began 30 min after [^{18}F]FDG infusion. Attenuation and scatter correction data (5 mCi ^{57}Co rotating point source, 10-min duration) were acquired immediately after the emission scan using software supplied by the scanner manufacturer. Emission data were reconstructed as 3-D volumes (0.949×0.949 mm pixels, 1.212 mm slice thickness), including scatter and attenuation correction, using an iterative maximum a posteriori (MAP) algorithm (smoothing factor: β=0.15) provided by the scanner manufacturer (Fig. 1). Volumes were inspected visually using ASIPro microPET software (Siemens Preclinical Solutions) to ensure that the entire brain (including the cerebellum) was within the FOV.

Registration and intensity normalization

Registration of the MRI and microPET datasets required creation of a new rhesus monkey MRI atlas target. Using the iterative procedure described previously by Buckner and colleagues (2004), MR images from the eight sham-operated control animals were mutually co-registered while an average of their MR images was simultaneously matched to a pre-existing macaque (*Macaca fascicularis*) MRI template (Black et al., 2005). This average MRI then served as the common atlas representative target for all animals in the current study. All image transformations were computed using procedures written at Washington University School of Medicine running on Sun Solaris workstations. MRI and microPET datasets in DICOM and scanner-specific proprietary formats were first converted to Analyze floating-point format. Each animal's T1-weighted SPGR MRI was registered (12 parameter affine transform) to the common atlas representative target. The microPET volume was registered (rigid body transform) to each individual's (native space) SPGR using a previously described multi-modal algorithm (Rowland et al., 2005). MicroPET-to-atlas registration was then accomplished using the same transforms applied during SPGR-to-atlas registration. All datasets were then resampled to 0.5×0.5×0.5 mm voxels in atlas space. Visual inspection verified that each individual's microPET and MRI datasets were mutually co-registered and in a common atlas space (Fig. 1). Similar to Rilling and colleagues (2001, 2004), microPET volumes were normalized to obtain a mean whole brain (including cerebellum) radioisotope (RI) count of 5000 as a control for differential uptake of [^{18}F]FDG across animals. To normalize each dataset, 5000 was divided by the animal's mean whole brain RI count to arrive at an individual normalization scale factor. Each voxel in the microPET volume was then multiplied by this scale factor to create the normalized microPET volume. Accordingly, the present microPET measures represent relative as opposed to absolute estimates of regional glucose metabolism.

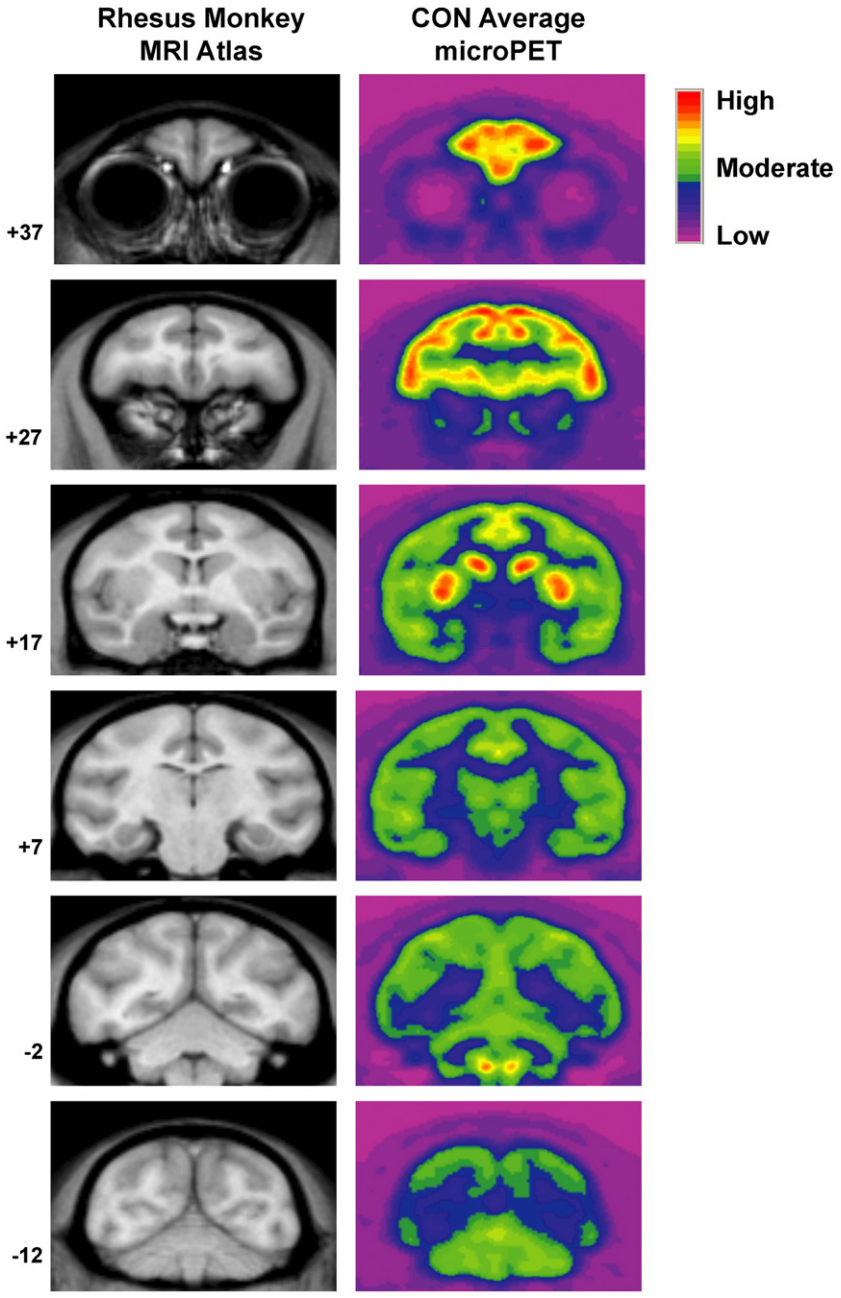

Fig. 1. Six coronal images, arranged from rostral (top) to caudal (bottom), are shown from the rhesus monkey MRI atlas created for MRI/microPET image registration (left column). Six registered microPET images representing the average glucose metabolism in the eight sham-operated control animals (CON) are also shown to demonstrate microPET image resolution and multi-modal spatial registration accuracy. On these, and all subsequent coronal MRI and microPET images, the observer's left is the animals left. Numbers to the left of each row represent the distance (in mm) of each image from the interaural plane. Colors indicating high, moderate and low glucose metabolism are indicated by the color bar.

Data analysis

Ordinarily, data analysis for this type of experiment would include whole-brain, voxel-wise comparisons (e.g., statistical parametric mapping (SPM) or three-dimensional stereotactic surface projection (3D-SSP)) to extract differences between the lesioned groups and control group. We initially used SPM5 software (Wellcome Department of Cognitive Neurology, Institute of Neurology, London) implemented in MATLAB R2006b (v. 7.3.0; The MathWorks, Inc., Natick, MA) to make pair-wise statistical comparisons between our three experimental groups. While this analysis revealed several significant differences, we questioned the reliability of those results for several reasons. First, as shown in Fig. 2, neurotoxic amygdala or hippocampus lesions typically produce significant local tissue atrophy and enlargement of the lateral ventricle's temporal horn consequent to the loss of neurons (Emery et al., 2001; Málková et al., 2001; Nemanic et al., 2002; Shelton et al., 2002; Bauman et al., 2004a,b, 2006). Also, for the amygdala-lesioned animals in the current study, injection needles penetrated the dorsal brain surface 4–5 times per

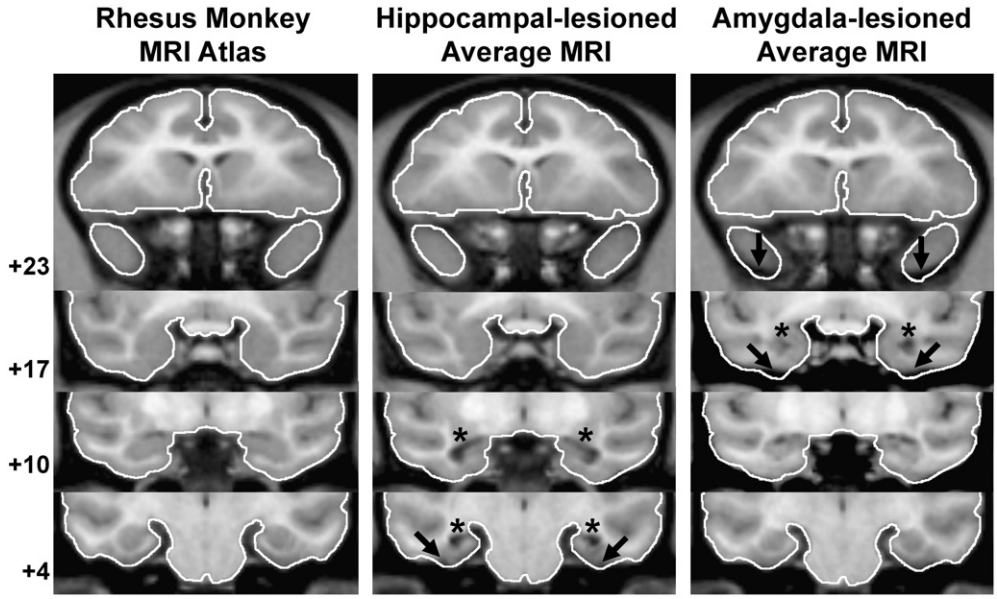

Fig. 2. Four coronal images, arranged from rostral (top) to caudal (bottom), are shown from the normalized rhesus monkey MRI atlas (left column), and averaged MRIs of all hippocampal-lesioned (center column) and amygdala-lesioned (right column) animals to demonstrate common areas of atrophied tissue (dark bands at arrow tips) or enlarged ventricles (dark areas below asterisks) in the lesioned animals. Numbers to the left of each row represent the distance (in mm) of each image from the interaural plane. The entire brain surface was traced in white on the four images from the rhesus monkey MRI atlas, and these boundaries were transferred directly onto registered images from the two lesioned groups. For the hippocampal-lesioned group, atrophied or shrunken tissue typically occurred around the parahippocampal cortex (level +4) and the temporal horns of the lateral ventricle are enlarged (levels +10 and +4). For the amygdala-lesioned animals, shrunken tissue typically occurred in the temporal pole, area TE, perirhinal cortex and entorhinal cortex (levels +23 and +17), and enlarged ventricles are also evident at level +17.

hemisphere within a 2 mm×2 mm square matrix en route to their neurotoxin delivery coordinates within the amygdala. This tight cluster of injections typically results in minor cortical distortions that also would not be present in sham-operated control animals. These systematic differences in gross brain structure between groups make it likely that in some regions, the same brain voxels are not compared across groups. We have chosen, therefore, to not include voxel-wise analyses in this report. Instead, we elected to take the more conservative approach of using a neuroanatomically-defined ROI analysis, thereby mitigating inter-animal differences in brain morphology.

Twenty distinct ROIs were individually defined (Analyze ROI tool) on each animal's T1-weighted MRI using anatomical landmarks. Fig. 3 shows each of these ROIs on sample coronal MR images from the rhesus monkey atlas target used for cross-modal image registration. A detailed description of the specific landmarks that served as boundaries for each ROI is provided in Supplementary Material online. The 20 ROIs were drawn manually on sections at 0.5 mm intervals by one rater (CJM). All ROIs, except the cerebellum, were drawn on coronal images and defined separately in the left and right hemispheres. Sagittal images were used for drawing the cerebellum ROI. For cortical ROIs, the tracings included all cortical layers and the ROI limit was at the border of the cortex and underlying white matter.

Each animal's ROI map was transferred onto their registered microPET volume and the average RI count within each ROI was measured using the Analyze ROI tool. Sham-operated controls did not demonstrate any significant differences in average RI counts across hemispheres for any ROI (paired-sample *t*-tests, all $p > .05$), and since lesion extent was highly symmetrical in both lesioned groups (see Results), all between groups statistical comparisons were conducted with RI counts averaged across hemispheres for each ROI. The distribution of mean RI counts for each ROI was then assessed for normality using the Shapiro–Wilk test, and inspection of the skewness and kurtosis ratios. From this analysis, data from the following five ROIs were found not to be normally distributed for one or more groups: Substantia innominata, caudate nucleus, parahippocampal cortex, hippocampus and temporal pole. Therefore, all data were $\log_{10}(x+1)$ transformed prior to group-wise comparisons. All ROIs, except for the cerebellum, were chosen based on known monosynaptic connections with the amygdala and/or hippocampus. We hypothesized that these ROIs would be hypometabolic in the lesioned groups, and therefore performed between groups comparisons with one-tailed independent samples *t*-tests. The cerebellar ROI was originally included in the study for the purposes of RI count normalization. However, group differences were detected for this ROI (see Results), which led to using the mean whole brain RI count as the basis for microPET normalization. Since there are no known monosynaptic connections between the cerebellum and amygdala or hippocampus in macaque monkeys, we could not make an *a priori* prediction as to the direction of any lesion-induced changes. Data for the cerebellum were therefore analyzed with two-tailed independent samples *t*-tests. For all ROIs, the following three comparisons were performed: CON vs. AMY, CON vs. HIP and AMY vs. HIP. Statistical significance was set at $p < .05$.

To visualize areas of significantly altered glucose metabolism, MRI/microPET fusion images (see Figs. 5, 7, 9 and 11) were created with the Subtraction Ictal SPECT CO-registered to MRI (SISCOM) module within the Analyze software package.

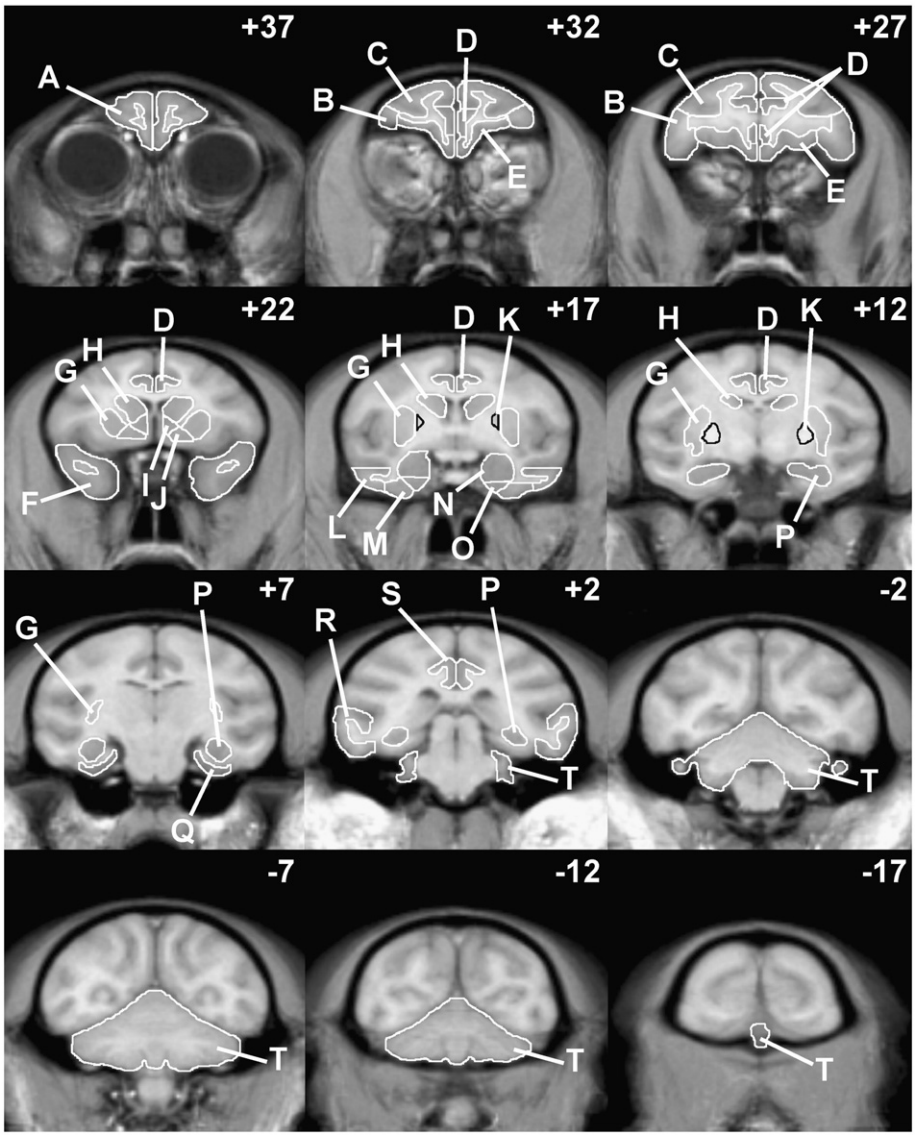

Fig. 3. Coronal images, arranged from rostral (top, left) to caudal (bottom, right), from the rhesus monkey MRI atlas are shown with the 20 ROIs used in this study. These sample images are spaced 5 mm apart, and their distance (in mm) from the interaural plane is given in the upper-right corner of each image. The following ROIs were drawn: (A) frontal pole, (B) ventrolateral prefrontal cortex, (C) dorsolateral prefrontal cortex, (D) anterior cingulate cortex, (E) orbital and ventromedial frontal cortex, (F) temporal pole, (G) putamen, (H) caudate nucleus, (I) nucleus accumbens, (J) substantia innominata, (K) globus pallidus, (L) area TE, (M) perirhinal cortex, (N) amygdala, (O) entorhinal cortex, (P) hippocampus, (Q) parahippocampal cortex, (R) area TEO, (S) retrosplenial cortex and (T) cerebellum.

microPET datasets were first averaged within each group using the Analyze Image Calculator tool. Within SISCOM, each group's averaged microPET dataset was subtracted from similar averages of the other two groups (i.e., CON–AMY, CON–HIP, AMY–CON, AMY–HIP, HIP–CON and HIP–AMY) using cubic spline interpolation. Voxel clusters that differed in RI count by more than two standard deviations were highlighted in orange. The microPET difference maps were then fused onto the rhesus monkey MRI atlas target and used for illustration purposes only.

Pearson product moment correlation matrices were also generated for ROIs demonstrating significant group differences to determine if the amount of hippocampal or amygdaloid tissue atrophy (averaged across hemispheres) was significantly related to the average RI count in those ROIs.

Results

Lesion extent

A qualitative evaluation of lesion extent using post-surgical T2-weighted MR images has been previously reported for the eight amygdala-lesioned and eight hippocampal-lesioned animals (Bauman et al., 2004a, 2006). Briefly, inspection of the hyperintense signal (indicating localized edema) visible on these images acquired 10 days after surgery showed that ibotenic acid injections were well focused in the amygdala or hippocampus of the respective cases. Hypersignal was also present in the parahippocampal cortex of hippocampal-lesioned animals, as well as the ventral claustrum, ventral putamen and anterior tip of the hippocampus for amygdala-lesioned animals.

Although T2-weighted MR images acquired soon after surgery provide confirmation of lesion placement and correlate positively with the extent of neuronal loss, they tend to overestimate the amount of damage observed during histological analysis (Málková et al., 2001; Nemanic et al., 2002; Shelton et al., 2002). Therefore, we also measured hippocampal and amygdala volume reductions in HIP and AMY using T1-weighted MR images acquired 4 years post-surgery (Table 1). This method of lesion analysis likely underestimates the actual damage. In adult cases for which we have histological information, the tissue that remains in the amygdala (Emery et al., 2001) or hippocampus (Banta-Lavenex et al., 2006) following neurotoxin injections is composed mostly of glial cells and fibers, rather than neurons.

The eight AMY animals demonstrated substantial, bilateral tissue atrophy in the area normally occupied by the amygdala, along with expansion of the temporal horn of the lateral ventricle. Compared to the average volume in sham-operated animals, amygdala volumes for AMY animals were reduced by 67.0–80.7%. The amygdala lesions were also highly symmetrical; volume reduction averaged 70.6% and 73.1% in the left and right hemispheres, respectively. Sparing of the amygdala typically occurred towards its caudal extreme, which lies dorsal to the anterior tip of the hippocampus. Unintended atrophy was visible in the rostral 1/4 of the hippocampus, resulting in a 26.7% reduction in hippocampal volume on average for AMY.

Significant hippocampal atrophy was also observed on the T1-weighted MR images of HIP. Relative to control animals, average hippocampal volume was reduced by 76.6% (range: 66.0–86.8%) in HIP animals. Lesions for HIP were also quite symmetrical; volume reduction averaged 78.0% and 75.2% in the left and right hemispheres, respectively. Sparing of the hippocampus typically only occurred at the rostral tip. Unintended amygdala atrophy was minor in the eight HIP cases, averaging only 14.6% for the group (range: 0–35.4%). Moderate tissue atrophy was also observed in the parahippocampal cortex for several cases, which precluded measurement of relative glucose metabolism in this ROI for HIP.

Table 1
Lesion extents for animals with amygdala or hippocampal lesions

AMY cases	Amygdala			Hippocampus		
	L	*R*	Avg	*L*	*R*	Avg
33329	57.9	76.2	67.0	49.4	46.1	47.8
33348	67.6	70.7	69.2	11.9	16.6	14.3
33412	69.1	74.7	71.9	14.4	17.8	16.1
33446	81.1	80.4	80.7	25.6	30.7	28.2
33449	67.3	71.8	69.5	13.6	18.8	16.2
33492	73.5	61.4	67.4	17.2	8.0	12.6
33495	72.5	74.2	73.4	41.6	26.4	34.0
33520	76.1	75.5	75.8	50.1	39.1	44.6
X	70.6	73.1	71.9	28.0	25.4	26.7
HIP cases	**Hippocampus**			**Amygdala**		
	L	*R*	Avg	*L*	*R*	Avg
33069	83.3	74.0	78.6	3.5	7.7	5.6
33205	79.0	71.4	75.2	0	0	0
33258	79.9	81.9	80.9	11.2	5.1	8.2
33355	86.0	87.7	86.8	35.8	35.0	35.4
33416	81.7	88.3	85.0	0	11.1	5.2
33425	70.6	61.4	66.0	10.8	4.5	7.6
33485	71.8	69.2	70.5	30.4	29.8	30.1
33503	72.2	68.1	70.2	33.0	25.6	29.3
X	78.0	75.2	76.6	14.9	14.2	14.6

Data are the percent reduction (or atrophy) of amygdaloid or hippocampal tissue for each case relative to mean sham-operated control volumes ($n=8$) for each structure. Volumes for the amygdala and hippocampus (in mm^3) were measured from T1-weighted MR images collected approximately 4 years after lesion or sham surgeries. *L*—percent volume reduction in the left hemisphere; *R*—percent volume reduction in the right hemisphere; Avg—average of *L* and *R*; *X*—group mean.

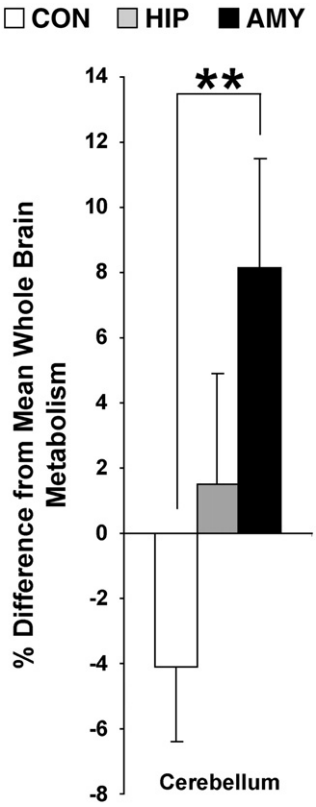

Fig. 4. Relative metabolism in the cerebellar ROI for each group. In this and all subsequent bar graphs, relative metabolism is displayed in terms of the percent difference from whole brain mean RI count (5000), and was calculated as follows: % Difference = ((mean ROI RI count − 5000)/5000) × 100. Vertical lines associated with each bar represent the standard error of the mean. $^{**}p<.01$.

Group demographics and microPET scan variables

The age at time of lesion surgery, as well as age and weight at time of microPET scan were compared between groups. Of these variables, CON was slightly older than AMY at the time of microPET scan (4.3 and 4.1 years respectively; $t=2.189$, $p<.05$). Several variables that could have potentially impacted the quality of each animal's microPET data were also examined. There were no significant group differences in average serum glucose concentration just prior to microPET imaging, average injected dose of [^{18}F]FDG (mCi) or average volume (ml) of [^{18}F]FDG injected (all $p>.10$). Finally, the groups did not differ appreciably in their whole brain mean RI count prior to normalization or in their normalization scale factors (all $p>.10$).

Relative glucose metabolism within defined ROIs

Cerebellum

Analysis of the cerebellar ROI revealed a significant difference between the groups (Figs. 4 and 5). AMY displayed greater glucose metabolism in this ROI than CON [$t=-3.013$, $p<.01$], but HIP did not differ from either group.

Frontal lobe

Several group differences were detected within the frontal lobe (Figs. 6 and 7). Specifically, AMY showed significantly lower metabolism in the orbital and ventromedial frontal cortex [$t=1.887$, $p<.05$] and in the anterior cingulate cortex [$t=1.924$, $p<.05$] relative to CON. Also, AMY showed significantly lower metabolism in the dorsolateral prefrontal cortex relative to CON [$t=2.345$, $p<.05$]. For all frontal lobe ROIs, HIP did not differ appreciably from any group.

Subcortical regions

Group differences were only detected for the caudate nucleus and putamen (Figs. 8 and 9). AMY displayed significantly lower metabolism relative to CON for both of these subcortical structures [caudate nucleus: $t=2.281$, $p<.05$, putamen: $t=2.289$, $p<.05$]. Again, HIP did not differ from either group in any subcortical ROI.

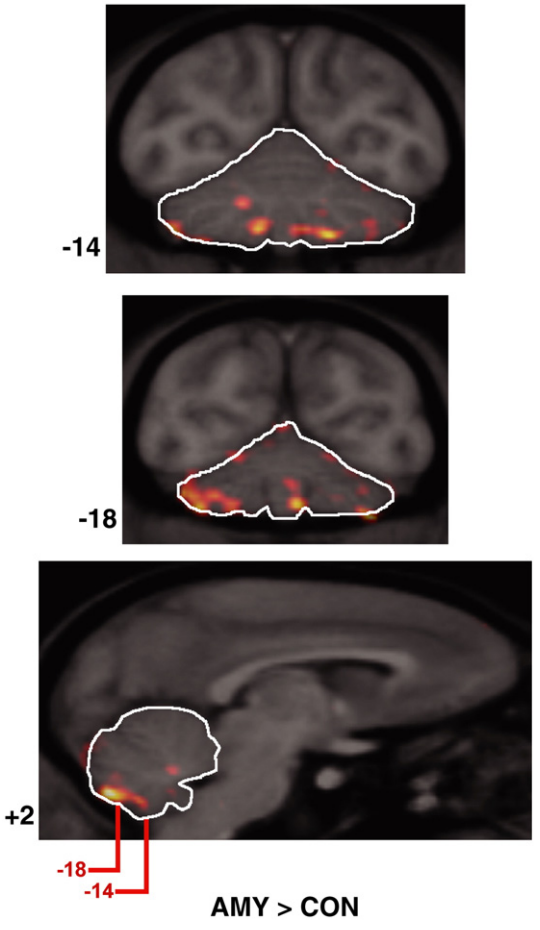

Fig. 5. Two coronal and one sagittal MRI/microPET fusion images with the cerebellar ROI outlined. Numbers to the left of coronal images indicate distance (in mm) from the interaural plane, whereas the number to the left of the sagittal image indicates distance (in mm) from the midsagittal plane (positive numbers indicate right hemisphere). The levels of the two coronal images are also indicated in red on the sagittal image. The orange overlay indicates areas where average RI count was more than two standard deviations greater in amygdala-lesioned animals relative to controls.

Temporal and posterior cingulate areas

Group differences were detected for two ROIs in the temporal and posterior cingulate cortices (Figs. 10 and 11). AMY displayed significantly lower metabolism in the hippocampus relative to CON [$t=3.448$, $p<.01$]. Because of their lesion, this ROI was not measured for HIP. A significant group difference was also found in the retrosplenial cortex. However, in this case, HIP demonstrated lower metabolism relative to CON [$t=2.323$, $p<.05$], but AMY did not differ from any group.

Correlations

Only one significant correlation was found between average RI count and the average amount of amygdaloid or hippocampal tissue atrophy. For AMY, there was a significant negative correlation between hippocampal atrophy and average RI count in the hippocampus ROI ($r=-.851$, $p<.01$).

Discussion

The current study is the first to report long-term changes in resting brain metabolism in the rhesus monkey following neonatal damage to the amygdala or hippocampus. Changes in resting brain glucose metabolism were more substantial after neonatal amygdala lesions compared to hippocampus lesions. Analysis of discrete, anatomically-based ROIs indicated that, relative to sham-operated controls, amygdala-lesioned animals displayed hypometabolism in the orbital and ventromedial frontal cortex, anterior cingulate cortex, dorsolateral prefrontal cortex, caudate nucleus, putamen and hippocampus and hypermetabolism in the cerebellum. In contrast, hippocampal-lesioned animals only displayed hypometabolism in the retrosplenial cortex relative to control animals.

Neonatal amygdala lesions and resting brain metabolism

Several of the findings for amygdala-lesioned animals are consistent with our predictions based on the known neuroanatomical connections of the amygdaloid complex (Amaral et al., 1992). Hypometabolism was detected in the orbital and ventromedial prefrontal cortex, anterior cingulate cortex, caudate nucleus, putamen and hippocampus. Each of these cortical and subcortical regions has substantial connections with the amygdala, especially the lateral, basal and accessory basal nuclei (Amaral et al., 1992; Stefanacci and Amaral, 2000; Shelton et al., 2002; Ghashghaei et al., 2007). These results also parallel a recent autoradiography study of cerebral glucose metabolism in adult rats that received ibotenic acid amygdala lesions as neonates (Gerrits et al., 2006). Relative to sham-operated rats, hypometabolism was detected in the anterior and posterior cingulate cortex, olfactory tubercle, anterior caudate and putamen, diagonal band of Broca, lateral septum, anterior hippocampus and thalamus. The specific cellular mechanisms underlying such regional changes in glucose metabolism following lesions are not known, but likely stem from a combination of factors. Since glucose metabolism measured with [^{18}F]FDG PET imaging reflects local integrated synaptic activity (Sokoloff, 1999; Rocher et al., 2003), a simple loss of excitatory or inhibitory input from the amygdala may be the most likely cause of the hypometabolism. The ability to acquire compensatory inputs or

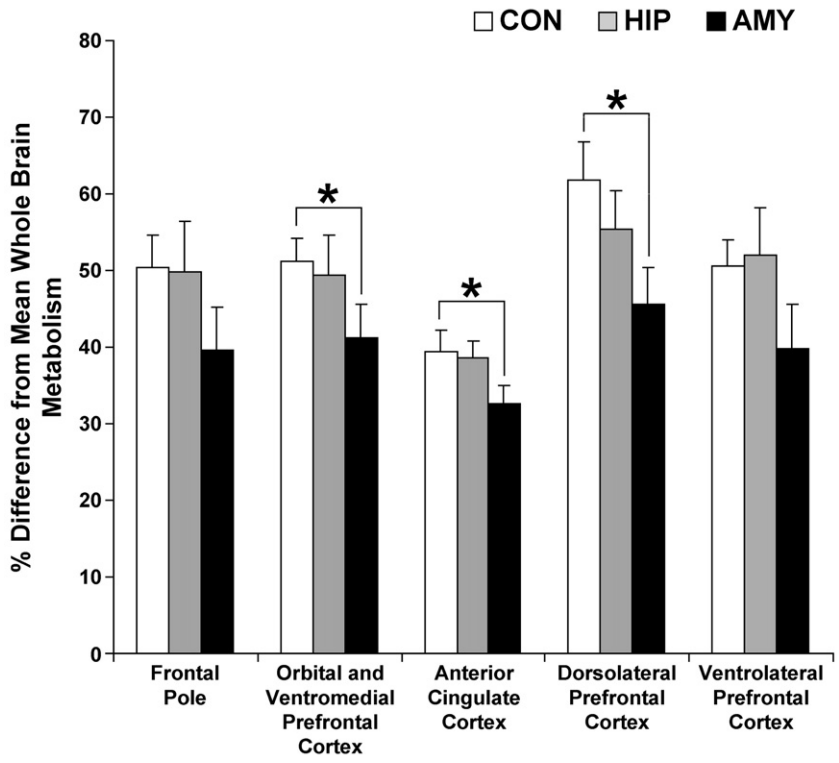

Fig. 6. The percent difference from mean whole brain metabolism in the five frontal lobe ROIs for each experimental group. For each ROI, the percent difference shown is an average across the left and right hemispheres. Group differences were detected for the orbital and ventromedial frontal cortex, anterior cingulate cortex and the dorsolateral prefrontal cortex, but not the frontal pole or ventrolateral prefrontal cortex. Vertical lines associated with each bar represent the standard error of the mean. *$p \leq .05$.

preserve those normally pruned during development may also differ from region to region. Finally, the loss of extrinsic connections may also dysregulate a region's intrinsic circuitry, further amplifying long-term metabolic changes. Regardless of mechanism, it appears that compensatory mechanisms in the developing rat and monkey brains are not sufficient to yield normal resting

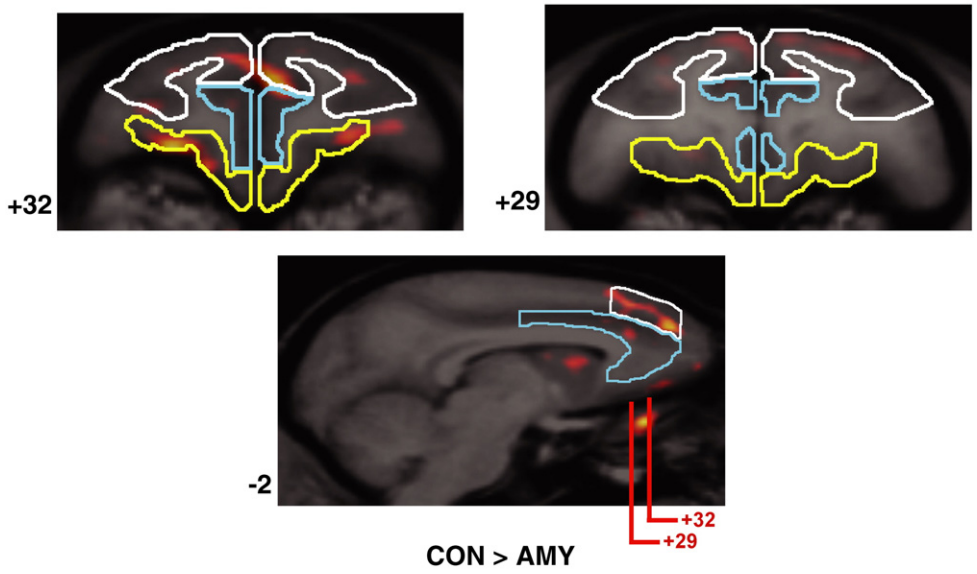

Fig. 7. Two coronal and one sagittal MRI/microPET fusion images are shown through the frontal lobes with the dorsolateral prefrontal cortex (white), anterior cingulate cortex (blue) and orbital and ventromedial frontal cortex (yellow) ROIs outlined. Numbers to the left of each image indicate distance (in mm) from the interaural plane for coronal images or from the midline for sagittal images (negative numbers indicate left hemisphere). The levels of the two coronal images are also indicated in red on the sagittal image. The orange overlay indicates areas where average RI count was more than two standard deviations greater in control animals than amygdala-lesioned animals.

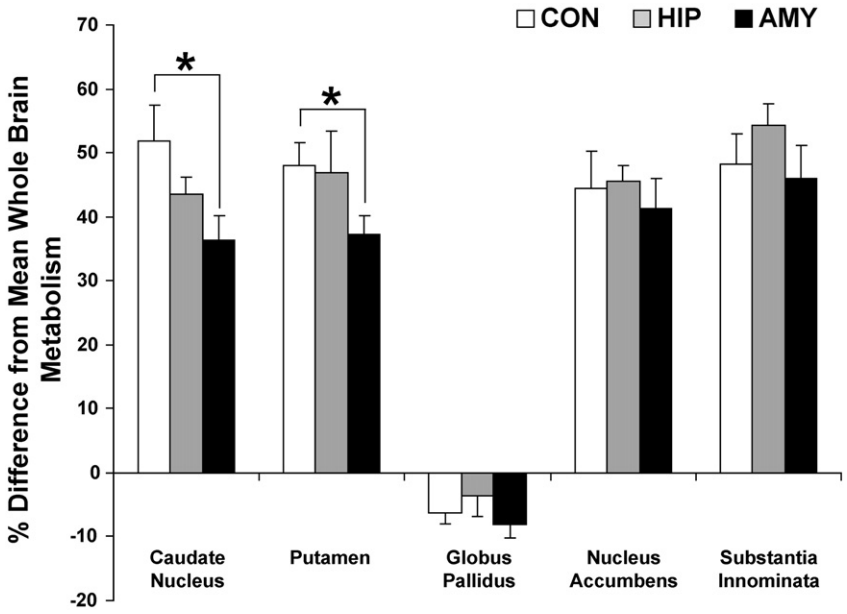

Fig. 8. The percent difference from mean whole brain metabolism in the five subcortical ROIs (averaged across hemispheres) for each experimental group. Significant group differences were detected for the caudate nucleus and putamen, but not for the globus pallidus, nucleus accumbens or substantia innominata. Vertical lines associated with each bar represent the standard error of the mean. $*p \leq .05$.

metabolism following a neonatal amygdala lesion, even if brain function is measured well into adulthood.

Beyond a loss of connections, it is also possible that hypometabolism in structures adjacent to the amygdala, such as the putamen and hippocampus, resulted from passage of neurotoxin injection needles and/or diffusion of neurotoxin delivered to the amygdala. Histological lesion assessment has not been completed for the amygdala-lesioned group due to continued behavioral and microPET studies. However, one of the amygdala-lesioned animals studied here (case 33329) died of causes unrelated to the lesion. Examination of Nissl-stained coronal tissue sections in the vicinity of this animal's lesion did not show any damage or gliosis in the putamen from passage of neurotoxin injection needles. Minor cell loss due to unintended diffusion of ibotenic acid was evident in the ventral tip of the claustrum and putamen bilaterally, but only extended 1–2 mm lateral and posterior to the central nucleus of the amygdala. However, this portion of the ventral putamen was not included in the putamen ROI, due to the difficulty of differentiating it from the amygdala on MR images (see Supplementary Material online). If this case is representative of the group, it is unlikely that inadvertent damage to the putamen was responsible for the overall hypometabolism of this structure.

Cell loss was also evident for this animal in the anterior 4 mm of the dentate gyrus and the CA fields of the hippocampus bilaterally, but was mostly confined to the lateral half of these areas. T1-weighted MR images collected 4 years post-surgery for this case showed an average of 47.8% reduction in hippocampal volume (see Table 1), the highest reduction for all amygdala-lesioned animals. Although the amygdala-lesioned group as a whole showed less average hippocampal atrophy across hemispheres (26.7%), we detected a significant negative correlation between hippocampal atrophy and mean hippocampal RI count. This implies that increased collateral damage to the hippocampus was related to lower mean metabolism in this structure. These factors indicate that the reduced hippocampal metabolism found for amygdala-lesioned animals may have been due both to loss of

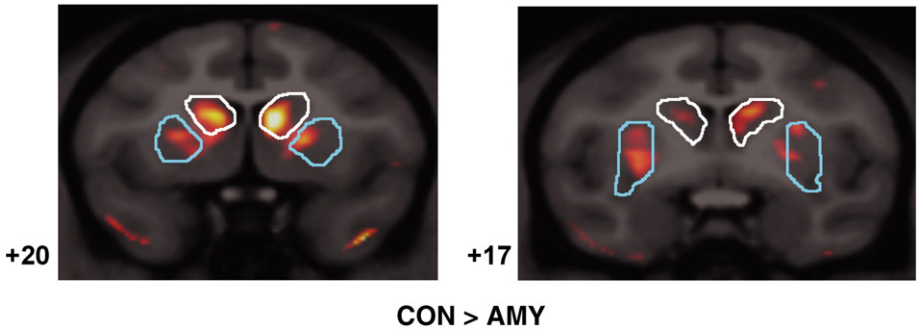

Fig. 9. Two coronal MRI/microPET fusion images are shown with the caudate nucleus (white) and putamen (blue) ROIs outlined. Numbers to the left of each image indicate distance (in mm) from the interaural plane. The orange overlay indicates areas where average RI count was more than two standard deviations greater in control animals than amygdala-lesioned animals.

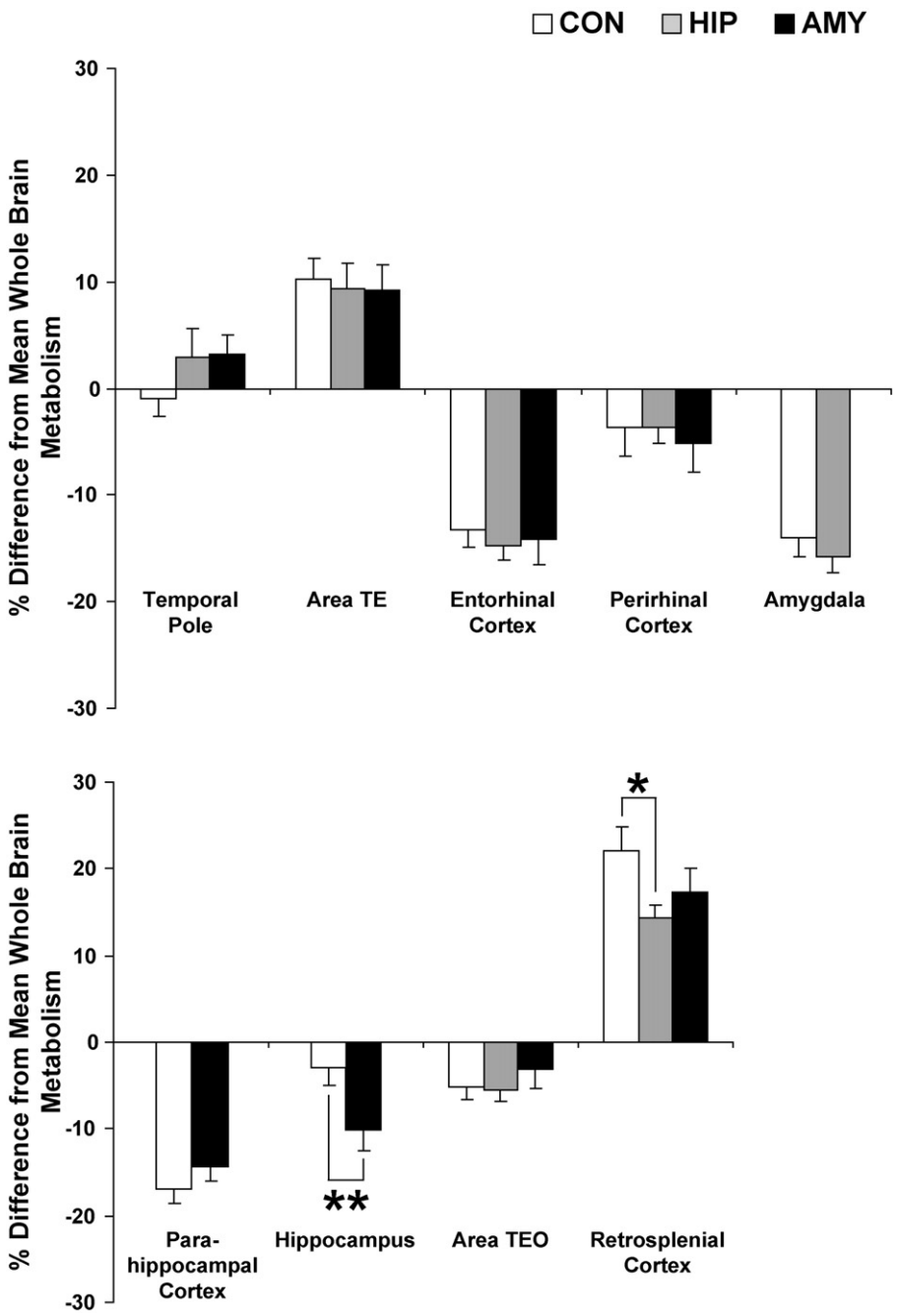

Fig. 10. The percent difference from mean whole brain metabolism in the nine temporal and posterior cingulate ROIs (left and right hemispheres averaged) for each experimental group. Significant group differences were only detected for the hippocampus and retrosplenial cortex. Vertical lines associated with each bar represent the standard error of the mean. $*p \leq .05$, $**p < .01$.

amygdaloid inputs and unintended damage of the anterior hippocampus.

Two findings for amygdala-lesioned animals were unexpected based on the amygdala's known connectivity. First, amygdala-lesioned animals displayed hypometabolism in the dorsolateral prefrontal cortex, an area with which the amygdala shares only light connections (Amaral et al., 1992; Ghashghaei et al., 2007). However, other evidence points to a stronger functional relationship between the medial temporal lobe and the prefrontal cortex. Bertolino and colleagues (1997) used *in vivo* proton magnetic resonance spectroscopy to measure relative amounts of *N*-acetyl-aspartate (NAA; a marker of neuronal viability) in the prefrontal cortex of rhesus monkeys that received large medial temporal lobe ablations (including the amygdala, hippocampus, entorhinal cortex and parahippocampal cortex) either as infants or as adults. Animals with neonatal medial temporal lobe lesions displayed decreased levels of NAA in the prefrontal cortex relative to both normal controls and animals that received similar lesions as adults. In a follow-up study with a subset of these same animals, Saunders and colleagues (1998) demonstrated that neonatal, but not adult medial

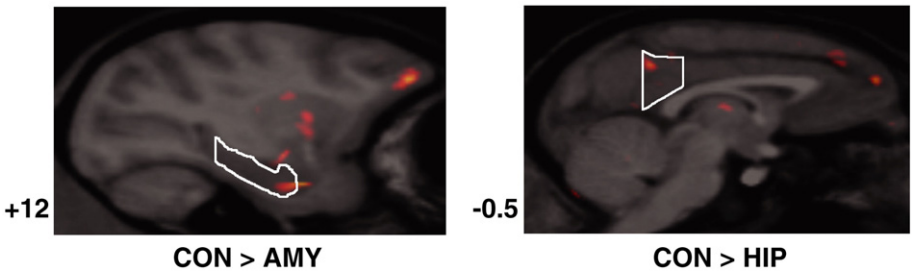

Fig. 11. Sagittal MRI/microPET fusion images showing the right hippocampus (left panel) and left retrosplenial cortex ROIs (right panel). Numbers to the left of these sagittal images indicate distance (in millimeters) from the midline (positive numbers indicate right hemisphere, negative numbers indicates left hemisphere). The orange overlay indicates areas where average RI count differed by more than two standard deviations between groups as indicated.

temporal lobe ablations disrupted the manner in which the dorsolateral prefrontal cortex regulates dopamine release by the caudate nucleus. Our findings are certainly in accord with these two previous studies, since animals with selective neonatal amygdala lesions demonstrated lower resting glucose metabolism in the orbital and medial frontal cortex, dorsolateral prefrontal cortex and caudate nucleus. Further, given that we found far more substantial changes in resting glucose metabolism in the frontal cortex and caudate nucleus for amygdala-lesioned animals compared to hippocampus-lesioned animals, the profound changes in prefrontal cortex neuronal viability and regulation of striatal dopamine release reported earlier for animals with large medial temporal lobe ablations may have been predominantly due to their amygdala damage.

A second interesting and unexpected finding was hypermetabolism within the cerebellum for amygdala-lesioned animals. Although the amygdala does not share any direct, monosynaptic connections with the cerebellum in nonhuman primates, the recent use of rabies virus as a transneuronal anatomical tracer has indicated multi-synaptic connections between the cerebellum and the prefrontal cortex (especially the dorsolateral prefrontal cortex, Kelly and Strick, 2003), and also between the cerebellum and putamen (Hoshi et al., 2005). It is possible that neonatal amygdala damage could influence metabolism in the cerebellum through these intermediary structures, since the amygdala possesses light, bidirectional connections with the dorsolateral prefrontal cortex and unidirectional connections with the putamen (Amaral et al., 1992; Ghashghaei et al., 2007), and both were significantly hypometabolic for amygdala-lesioned animals.

Is it possible that the cerebellar hypermetabolism is an artifact of the microPET normalization process? Forcing all microPET datasets to have an equal whole brain mean RI count was necessary to control for differential uptake of [^{18}F]FDG across animals. Since the amygdala-lesioned group displayed at least six regions of hypometabolism, their average whole brain RI count may have been significantly lower than the other groups. Likewise, the normalization scale factors for this group may have been disproportionately larger than the other two experimental groups. If this were the case, our microPET normalization method could artificially inflate RI counts in the amygdala-lesioned animals more than the other groups, thus producing hypermetabolism that did not truly exist. However, this possibility is unlikely since none of the experimental groups differed significantly in mean whole brain RI counts prior to normalization (all $ps > .10$) or average normalization scale factor (all $ps > .10$). Furthermore, other variables that could have affected each group's microPET dataset, such as blood glucose concentration prior to microPET imaging and strength of [^{18}F]FDG dose, did not differ appreciably between groups (all $ps > .10$). Therefore, it is unlikely that any of these factors influenced the results presented here.

Since this experiment occurred more than 4 years after surgery, each of the alterations in glucose metabolism for amygdala-lesioned animals likely represent stable and permanent changes in resting brain function. Although the social and emotional development of these animals have been extensively chronicled (Bauman et al., 2004a,b, 2006), it is difficult to speculate about how the metabolic alterations described here may have combined with amygdala damage to result in behavioral differences from sham-operated control animals. In the current study, [^{18}F]FDG uptake occurred while the animals were anesthetized with ketamine and isoflurane rather than during a behavioral task. Additionally, no formal behavioral measures were collected from these animals in close temporal proximity to the current experiment. Given these factors, our study may be more closely related to recent human and monkey functional magnetic resonance imaging (fMRI) studies of resting state activity. Such studies have provided compelling evidence for a "default system" of brain activity that predominates in the absence of any overt cognitive demand or goal-directed behavioral task (Gusnard et al., 2001; Raichle et al., 2001). In the human brain, these areas include the posterior cingulate cortex, retrosplenial cortex, lateral parietal cortex, medial prefrontal cortex, superior frontal gyrus, inferior temporal gyrus, parahippocampal gyrus, and the cerebellar tonsils (Fox et al., 2005). In humans, heightened default system activity has been linked to complex cognitive processes, such as theory of mind (Saxe and Kanwisher, 2003), moral reasoning (Greene et al., 2001), active self-referential behavior (Vogeley and Fink, 2003), recollection (Wagner et al., 2005) and imagining the future (Addis et al., 2007). Recently, Vincent and colleagues (2007) demonstrated with fMRI that many elements of this default system are present in the anesthetized macaque monkey brain. In the current study, we found that neonatal amygdala lesions resulted in hypermetabolism in the cerebellum and hypometabolism in the lateral and medial prefrontal cortices of anesthetized monkeys. Could this mean that monkeys with neonatal amygdala lesions also have a defective default system of brain activity? These findings suggest an exciting direction for future research.

Neonatal hippocampus lesions and resting brain metabolism

Significant long-term metabolic effects of neonatal hippocampus lesions were much less apparent than neonatal amygdala lesions. This finding is consistent with the recent autoradiographic study discussed above by Gerrits and colleagues (2006). In that

study, rats that received neurotoxic ventral hippocampus lesions soon after birth did not show any changes in glucose metabolism outside the lesion site as adults. Our study did find one region of altered metabolism following neonatal hippocampus lesions in monkeys, the retrosplenial cortex. This novel finding is consistent with existing neuroanatomical data showing that the hippocampal formation, especially the subiculum, is heavily interconnected with the retrosplenial cortex (Kobayashi and Amaral, 2003). A topographically similar connection between the hippocampus and retrosplenial cortex has also been seen in the correlation structure of functional neuroimaging signals in humans (Vincent et al., 2006). It is again interesting to note that the human and monkey retrosplenial cortex has been implicated as part of the default system of brain activity (Fox et al., 2005; Vincent et al., 2007). Hypometabolism in this region following neonatal hippocampus lesions might again imply that these animals have a somewhat defective pattern of brain activity while at rest. The exact behavioral repercussions of such an abnormality are again unknown, but certainly warrant future study.

It was surprising that alterations in the resting metabolism of other regions robustly connected to the hippocampus (e.g., amygdala, nucleus accumbens and entorhinal cortex) were not detected. One explanation for this negative result is that compensatory structural and functional reorganization was more successful in these regions. This is plausible, since a recent study from our laboratory with these same neonatal hippocampus-lesioned animals demonstrated preserved allocentric spatial relational learning (Lavenex et al., 2007), whereas hippocampus lesions produced during adulthood prevented learning in the same task (Banta-Lavenex et al., 2006). A second possibility is that metabolic deficits in some hippocampal target structures may not be detectable by microPET scans if uptake of the [^{18}F]FDG occurred while animals were under general anesthesia. If heightened activity in the primate medial temporal lobe memory system (including the hippocampus, entorhinal cortex, perirhinal cortex and parahippocampal cortex) reflects the encoding and retrieval of information (Schacter and Wagner, 1999; Tulving et al., 1999), then this system may be metabolically indistinguishable in normal and hippocampal-lesioned monkeys when they are sedated. Therefore, abnormal activity patterns may be more apparent for hippocampal-lesioned animals if metabolic data were acquired following behavioral or cognitive tasks that require encoding or retrieval of spatial or semantic information.

Implications for developmental lesion studies

The results presented here also have broad implications for the interpretation of longitudinal lesion studies in nonhuman primates, especially those targeting the complex neural networks underlying social behavior, emotion and memory. These abilities are crucial for the survival of group-living primates and require the concerted operation of many brain regions that span the perceptual, cognitive and motor domains. It is apparent from the current study that focal damage to one node in a complicated neural network may have widespread and long lasting repercussions in other nodes. If alterations of resting glucose metabolism are any indication, the amount of dysregulation that occurs and the amount of functional reorganization that takes place may vary from node to node. This idea, unfortunately, complicates developmental lesion studies. For example, our laboratory is studying the role of the amygdala and hippocampus in the development of nonhuman primate social behavior and emotional reactivity using a combination of neonatal neurotoxic lesions and longitudinal behavioral analysis. Interpretation of such behavioral data is complicated by the current findings that neonatal amygdala or hippocampus lesions not only remove these structures from normal neural and behavioral development, but also change how other closely related structures function in a resting state. Thus, the present study highlights the perspective that the behavioral alterations in animals with neonatal lesions may be due to the intended damage, consequent brain reorganization or a combination of both. This should therefore be an important consideration when interpreting findings from lesion studies particularly when the lesion takes place in developing organisms.

Acknowledgments

This work was supported by funding from the National Institutes of Mental Health (2 R37 MH57502) to D. G. Amaral and was carried out, in part, at the California National Primate Research Center (RR00069). We thank the veterinary and animal services staff of the California National Primate Research Center for excellent care of the animals in this study. We also thank J. Bennett and P. Tennant for assistance with surgeries, S. Rendig and C. Griesemer for assistance in microPET image acquisition and reconstruction, as well as R. Larson for assistance in MR image acquisition. Finally, we would like to thank the two anonymous reviewers who offered valuable comments on a previous version of this paper.

References

Addis, D.R., Wong, A.T., Schacter, D.L., 2007. Remembering the past and imagining the future: common and distinct neural substrates during event construction and elaboration. Neuropsychologia 45, 1363–1377.

Alkire, M.T., Haier, R.J., Shah, N.K., Anderson, C.T., 1997. Positron emission tomography study of regional cerebral metabolism in humans during isoflurane anesthesia. Anesthesiology 86, 549–557.

Alvarado, M.C., Bachevalier, J., 2000. Revisiting the maturation of medial temporal lobe memory functions in primates. Learn. Mem. 7, 244–256.

Amaral, D.G., Price, J.L., Pitkänen, A., Carmichael, S.T., Aggleton, J.P., 1992. Anatomical organization of the primate amygdaloid complex. The Amygdala: Neurobiological Aspects of Emotion, Memory, and Mental Dysfunction. John Wiley and Sons, Inc., New York, pp. 1–66.

Banta-Lavenex, P., Amaral, D.G., Lavenex, P., 2006. Hippocampal lesion prevents spatial relational learning in adult macaque monkeys. J. Neurosci. 26, 4546–4558.

Bauman, M.D., Amaral, D.G., 2007. Neurodevelopment of social cognition. In: Nelson, C.A., Luciana, M. (Eds.), Handbook of Developmental Cognitive Neuroscience, vol. 2. MIT Press, Cambridge.

Bauman, M.D., Lavenex, P., Mason, W.A., Capitanio, J.P., Amaral, D.G., 2004a. The development of mother–infant interactions after neonatal amygdala lesions in rhesus monkeys. J. Neurosci. 24, 711–721.

Bauman, M.D., Lavenex, P., Mason, W.A., Capitanio, J.P., Amaral, D.G., 2004b. The development of social behavior following neonatal amygdala lesions in rhesus monkeys. J. Cogn. Neurosci. 16, 1388–1411.

Bauman, M.D., Toscano, J.E., Mason, W.A., Lavenex, P., Amaral, D.G., 2006. The expression of social dominance following neonatal lesions of the amygdala or hippocampus in rhesus monkeys (*Macaca mulatta*). Behav. Neurosci. 120, 749–760.

Bertolino, A., Saunders, R.C., Mattay, V.S., Bachevalier, J., Frank, J.A., Weinberger, D.R., 1997. Altered development of prefrontal neurons in rhesus monkeys with neonatal mesial temporo-limbic lesions: a proton

magnetic resonance spectroscopic imaging study. Cereb. Cortex 7, 740–748.

Black, K.J., Koller, J.M., Perlmutter, J.S., 2005. Template images for neuroimaging in *Macaca fascicularis*. Program No. 454.18. Neuroscience Meeting Planner. Society for Neuroscience, Washington, DC. Online.

Buckner, R.L., Head, D., Parker, J., Fotenos, A.F., Marcus, D., Morris, J.C., Snyder, A.Z., 2004. A unified approach for morphometric and functional data analysis in young, old, and demented adults using automated atlas-based head size normalization: reliability and validation against manual measurement of total intracranial volume. NeuroImage 23, 724–738.

Emery, N.J., Capitanio, J.P., Mason, W.A., Machado, C.J., Mendoza, S.P., Amaral, D.G., 2001. The effects of bilateral lesions of the amygdala on dyadic social interactions in rhesus monkeys (*Macaca mulatta*). Behav. Neurosci. 115, 515–544.

Fox, M.D., Snyder, A.Z., Vincent, J.L., Corbetta, M., Van Essen, D.C., Raichle, M.E., 2005. The human brain is intrinsically organized into dynamic, anticorrelated functional networks. Proc. Natl. Acad. Sci. U. S. A. 102, 9673–9678.

Freo, U., Ori, C., 2004. Effects of anesthesia and recovery from ketamine racemate and enantiomers on regional cerebral glucose metabolism in rats. Anesthesiology 100, 1172–1178.

Gerrits, M.A., Wolterink, G., van Ree, J.M., 2006. Cerebral metabolic consequences in the adult brain after neonatal excitotoxic lesions of the amygdala in rats. Eur. Neuropsychopharmacol. 16, 358–365.

Ghashghaei, H.T., Hilgetag, C.C., Barbas, H., 2007. Sequence of information processing for emotions based on the anatomic dialogue between prefrontal cortex and amygdala. NeuroImage 34, 905–923.

Goldman-Rakic, P.S., 1987. Development of cortical circuitry and cognitive function. Child Dev. 58, 601–622.

Greene, J.D., Sommerville, R.B., Nystrom, L.E., Darley, J.M., Cohen, J.D., 2001. An fMRI investigation of emotional engagement in moral judgment. Science 293, 2105–2108.

Gusnard, D.A., Raichle, M.E., Raichle, M.E., 2001. Searching for a baseline: functional imaging and the resting human brain. Nat. Rev., Neurosci. 2, 685–694.

Hayashi, T., Fukuyama, H., Katsumi, Y., Hanakawa, T., Nagahama, Y., Yamauchi, H., Tsukada, H., Shibasaki, H., 1999. Cerebral glucose metabolism in unilateral entorhinal cortex-lesioned rats: an animal PET study. NeuroReport 10, 2113–2118.

Heinz, A., Saunders, R.C., Kolachana, B.S., Jones, D.W., Gorey, J.G., Bachevalier, J., Weinberger, D.R., 1999. Striatal dopamine receptors and transporters in monkeys with neonatal temporal limbic damage. Synapse 32, 71–79.

Holcomb, H.H., Lahti, A.C., Medoff, D.R., Weiler, M., Tamminga, C.A., 2001. Sequential regional cerebral blood flow brain scans using PET with H2(15)O demonstrate ketamine actions in CNS dynamically. Neuropsychopharmacology 25, 165–172.

Honey, R.A., Honey, G.D., O'Loughlin, C., Sharar, S.R., Kumaran, D., Bullmore, E.T., Menon, D.K., Donovan, T., Lupson, V.C., Bisbrown-Chippendale, R., Fletcher, P.C., 2004. Acute ketamine administration alters the brain responses to executive demands in a verbal working memory task: an FMRI study. Neuropsychopharmacology 29, 1203–1214.

Hoshi, E., Tremblay, L., Feger, J., Carras, P.L., Strick, P.L., 2005. The cerebellum communicates with the basal ganglia. Nat. Neurosci. 8, 1491–1493.

Itoh, T., Wakahara, S., Nakano, T., Suzuki, K., Kobayashi, K., Inoue, O., 2005. Effects of anesthesia upon 18F-FDG uptake in rhesus monkey brains. Ann. Nucl. Med. 19, 373–377.

Katsumi, Y., Hanakawa, T., Fukuyama, H., Hayashi, T., Nagahama, Y., Yamauchi, H., Ouchi, Y., Tsukada, H., Shibasaki, H., 1999. The effect of sequential lesioning in the basal forebrain on cerebral cortical glucose metabolism in rats. An animal positron emission tomography study. Brain Res. 837, 75–82.

Kelly, R.M., Strick, P.L., 2003. Cerebellar loops with motor cortex and prefrontal cortex of a nonhuman primate. J. Neurosci. 23, 8432–8444.

Kobayashi, Y., Amaral, D.G., 2003. Macaque monkey retrosplenial cortex: II. Cortical afferents. J. Comp. Neurol. 466, 48–79.

Langsjo, J.W., Kaisti, K.K., Aalto, S., Hinkka, S., Aantaa, R., Oikonen, V., Sipila, H., Kurki, T., Silvanto, M., Scheinin, H., 2003. Effects of subanesthetic doses of ketamine on regional cerebral blood flow, oxygen consumption, and blood volume in humans. Anesthesiology 99, 614–623.

Langsjo, J.W., Salmi, E., Kaisti, K.K., Aalto, S., Hinkka, S., Aantaa, R., Oikonen, V., Viljanen, T., Kurki, T., Silvanto, M., Scheinin, H., 2004. Effects of subanesthetic ketamine on regional cerebral glucose metabolism in humans. Anesthesiology 100, 1065–1071.

Lavenex, P., Banta-Lavenex, P., Amaral, D.G., 2007. Spatial relational learning persists following neonatal hippocampal lesions in macaque monkeys. Nat. Neurosci. 10, 234–239.

Le Mestric, C., Chavoix, C., Chapon, F., Mezenge, F., Epelbaum, J., Baron, J.C., 1998. Effects of damage to the basal forebrain on brain glucose utilization: a reevaluation using positron emission tomography in baboons with extensive unilateral excitotoxic lesion. J. Cereb. Blood Flow Metab. 18, 476–490.

Machado, C.J., Bachevalier, J., 2003. Non-human primate models of childhood psychopathology: the promise and the limitations. J. Child Psychol. Psychiatry 44, 64–87.

Machado, C.J., Cherry, S.R., Snyder, A.Z., Amaral, D.G., 2006. Effects of amygdala or hippocampal lesions on resting brain metabolism in the macaque monkey. Program No. 488.9. Neuroscience Meeting Planner. Society for Neuroscience, Atlanta, GA. Online.

Maekawa, T., Tommasino, C., Shapiro, H.M., Keifer-Goodman, J., Kohlenberger, R.W., 1986. Local cerebral blood flow and glucose utilization during isoflurane anesthesia in the rat. Anesthesiology 65, 144–151.

Málková, L., Lex, C.K., Mishkin, M., Saunders, R.C., 2001. MRI-Based evaluation of locus and extent of neurotoxic lesions in monkeys. Hippocampus 11, 361–370.

Meguro, K., Blaizot, X., Kondoh, Y., Le Mestric, C., Baron, J.C., Chavoix, C., 1999. Neocortical and hippocampal glucose hypometabolism following neurotoxic lesions of the entorhinal and perirhinal cortices in the non-human primate as shown by PET. Implications for Alzheimer's disease. Brain 122 (Pt 8), 1519–1531.

Millien, I., Blaizot, X., Giffard, C., Mezenge, F., Insausti, R., Baron, J.C., Chavoix, C., 2002. Brain glucose hypometabolism after perirhinal lesions in baboons: implications for Alzheimer disease and aging. J. Cereb. Blood Flow Metab. 22, 1248–1261.

Moore, T.H., Osteen, T.L., Chatziioannou, T.F., Hovda, D.A., Cherry, T.R., 2000. Quantitative assessment of longitudinal metabolic changes in vivo after traumatic brain injury in the adult rat using FDG-microPET. J. Cereb. Blood Flow Metab. 20, 1492–1501.

Nemanic, S., Alvarado, M.C., Price, R.E., Jackson, E.F., Bachevalier, J., 2002. Assessment of locus and extent of neurotoxic lesions in monkeys using neuroimaging techniques: a replication. J. Neurosci. Methods 121, 199–209.

Noda, A., Takamatsu, H., Minoshima, S., Tsukada, H., Nishimura, S., 2003. Determination of kinetic rate constants for 2-[18F]fluoro-2-deoxy-D-glucose and partition coefficient of water in conscious macaques and alterations in aging or anesthesia examined on parametric images with an anatomic standardization technique. J. Cereb. Blood Flow Metab. 23, 1441–1447.

Ori, C., Dam, M., Pizzolato, G., Battistin, L., Giron, G., 1986. Effects of isoflurane anesthesia on local cerebral glucose utilization in the rat. Anesthesiology 65, 152–156.

Prather, M.D., Lavenex, P., Mauldin-Jourdain, M.L., Mason, W.A., Capitanio, J.P., Mendoza, S.P., Amaral, D.G., 2001. Increased social fear and decreased fear of objects in monkeys with neonatal amygdala lesions. Neuroscience 106, 653–658.

Raichle, M.E., MacLeod, A.M., Snyder, A.Z., Powers, W.J., Gusnard, D.A., Shulman, G.L., 2001. A default mode of brain function. Proc. Natl. Acad. Sci. U. S. A. 98, 676–682.

Rauchs, G., Blaizot, X., Giffard, C., Baron, J.C., Insausti, R., Chavoix, C.,

2006. Imaging visual recognition memory network by PET in the baboon: perirhinal cortex heterogeneity and plasticity after perirhinal lesion. J. Cereb. Blood Flow Metab. 26, 301–309.
Rempel-Clower, N.L., Zola, S.M., Squire, L.R., Amaral, D.G., 1996. Three cases of enduring memory impairment after bilateral damage limited to the hippocampal formation. J. Neurosci. 16, 5233–5255.
Rilling, J.K., Winslow, J.T., O'Brien, D., Gutman, D.A., Hoffman, J.M., Kilts, C.D., 2001. Neural correlates of maternal separation in rhesus monkeys. Biol. Psychiatry 49, 146–157.
Rilling, J.K., Winslow, J.T., Kilts, C.D., 2004. The neural correlates of mate competition in dominant male rhesus macaques. Biol. Psychiatry 56, 364–375.
Rocher, A.B., Chapon, F., Blaizot, X., Baron, J.C., Chavoix, C., 2003. Resting-state brain glucose utilization as measured by PET is directly related to regional synaptophysin levels: a study in baboons. NeuroImage 20, 1894–1898.
Rowland, D.J., Garbow, J.R., Laforest, R., Snyder, A.Z., 2005. Registration of [(18)F]FDG microPET and small-animal MRI. Nucl. Med. Biol. 32, 567–572.
Saunders, R.C., Kolachana, B.S., Bachevalier, J., Weinberger, D.R., 1998. Neonatal lesions of the medial temporal lobe disrupt prefrontal cortical regulation of striatal dopamine. Nature 393, 169–171.
Saxe, R., Kanwisher, N., 2003. People thinking about thinking people. The role of the temporo-parietal junction in "theory of mind". NeuroImage 19, 1835–1842.
Schacter, D.L., Wagner, A.D., 1999. Medial temporal lobe activations in fMRI and PET studies of episodic encoding and retrieval. Hippocampus 9, 7–24.
Shelton, S.E., Oakes, T.R., Kalin, N.H., 2002. Assessment of ibotenic acid amygdala lesions in monkeys using MRI. Program No. 404.7. Neuroscience Meeting Planner. Society for Neuroscience, Orlando, FL. Online.
Shimoji, K., Ravasi, L., Schmidt, K., Soto-Montenegro, M.L., Esaki, T., Seidel, J., Jagoda, E., Sokoloff, L., Green, M.V., Eckelman, W.C., 2004. Measurement of cerebral glucose metabolic rates in the anesthetized rat by dynamic scanning with 18F-FDG, the ATLAS small animal PET scanner, and arterial blood sampling. J. Nucl. Med. 45, 665–672.
Sokoloff, L., 1999. Energetics of functional activation in neural tissues. Neurochem. Res. 24, 321–329.
Stefanacci, L., Amaral, D.G., 2000. Topographic organization of cortical inputs to the lateral nucleus of the macaque monkey amygdala: a retrograde tracing study. J. Comp. Neurol. 421, 52–79.
Tai, C., Chatziioannou, A., Siegel, S., Young, J., Newport, D., Goble, R.N., Nutt, R.E., Cherry, S.R., 2001. Performance evaluation of the microPET P4: a PET system dedicated to animal imaging. Phys. Med. Biol. 46, 1845–1862.
Toyama, H., Ichise, M., Liow, J.S., Modell, K.J., Vines, D.C., Esaki, T., Cook, M., Seidel, J., Sokoloff, L., Green, M.V., Innis, R.B., 2004. Absolute quantification of regional cerebral glucose utilization in mice by 18F-FDG small animal PET scanning and 2–14C-DG autoradiography. J. Nucl. Med. 45, 1398–1405.
Tulving, E., Habib, R., Nyberg, L., Lepage, M., McIntosh, A.R., 1999. Positron emission tomography correlations in and beyond medial temporal lobes. Hippocampus 9, 71–82.
Vargha-Khadem, F., Gadian, D.G., Watkins, K.E., Connelly, A., Van Paesschen, W., Mishkin, M., 1997. Differential effects of early hippocampal pathology on episodic and semantic memory. Science 277, 376–380.
Vincent, J.L., Snyder, A.Z., Fox, M.D., Shannon, B.J., Andrews, J.R., Raichle, M.E., Buckner, R.L., 2006. Coherent spontaneous activity identifies a hippocampal–parietal memory network. J. Neurophysiol. 96, 3517–3531.
Vincent, J.L., Patel, G.H., Fox, M.D., Snyder, A.Z., Baker, J.T., Van Essen, D.C., Zempel, J.M., Snyder, L.H., Corbetta, M., Raichle, M.E., 2007. Intrinsic functional architecture in the anaesthetized monkey brain. Nature 447, 83–86.
Vogeley, K., Fink, G.R., 2003. Neural correlates of the first-person-perspective. Trends Cogn. Sci. 7, 38–42.
Wagner, A.D., Shannon, B.J., Kahn, I., Buckner, R.L., 2005. Parietal lobe contributions to episodic memory retrieval. Trends Cogn. Sci. 9, 445–453.
Zola, S.M., Squire, L.R., Amaral, D.G., 1986. Human amnesia and the medial temporal lobe region: Enduring memory impairment following a bilateral lesioin limited to the CA1 field of the hippocampus. J. Neurosci. 6, 2950–2967.